Crystal and magnetic structure of ferromagnetic superconducting $RuSr_2GdCu_2O_8$

O. Chmaissem
Department of Physics, Northern Illinois University, DeKalb, Illinois 60115
and Materials Science Division, Argonne National Laboratory, Argonne, Illinois 60439

J. D. Jorgensen, H. Shaked,* and P. Dollar
Materials Science Division, Argonne National Laboratory, Argonne, Illinois 60439

J. L. Tallon
Industrial Research Limited, P.O. Box 13130, Lower Hutt, New Zealand
(Received 20 August 1999)

The crystal and magnetic structure of a sample of $RuSr_2{}^{160}GdCu_2O_8$ which orders magnetically at 133 K and exhibits a superconducting transition at 35 K has been investigated by neutron powder diffraction. RuO_6 octahedra, which substitute at the chain copper site in a $YBa_2Cu_3O_7$-type structure, are rotated by about 14° around the *c* axis to accommodate physically reasonable Ru-O bond lengths in the plane. This results in a $\sqrt{2}a_p \times \sqrt{2}a_p \times c$ supercell. The RuO_6 rotations are partially ordered to form competing domains that differ in the sense of rotation. We speculate that the degree of ordering depends on annealing conditions. Surprisingly, the only structural parameters that respond to the magnetic ordering at 133 K are the Cu-Cu distance, which defines the thickness of the CuO_2 double layer, and the buckling angle of the CuO_2 planes. Magnetic scattering consistent with the previously proposed ferromagnetic ordering of Ru moments perpendicular to the *c* axis is not observed. We do not rule out ordering of Ru moments parallel to the *c* axis or itinerant ferromagnetism.

INTRODUCTION

A new class of hybrid ruthenocuprates, $RuSr_2LnCu_2O_8$ (Ru-1212) and $RuSr_2(Ln_{1+x}Ce_{1-x})Cu_2O_{10}$ (Ru-1222) (Ln = Sm, Eu, and Gd), was synthesized in 1995.[1] Ru-1212 is isostructural with $YBa_2Cu_3O_{7-\delta}$ (YBCO) with Y, Ba, and Cu1 (the chain copper atom) being completely replaced by Gd, Sr, and Ru, respectively. Although $RuSr_2GdCu_2O_8$ samples were not bulk superconductors, some trace of superconductivity was observed from resistance measurements. However, the superconductivity could not be unambiguously attributed to the 1212 phase.[1]

Later, Tallon *et al.*[2] found that, with special synthesis and annealing procedures, $RuSr_2GdCu_2O_8$ can be made ferromagnetic ($T_M \sim 133$ K) and superconducting (T_C up to 46 K) with a Meissner fraction close to 100% at 4.2 K. Several measurements have been performed to confirm the coexistence of superconductivity and ferromagnetism, below T_C, in this material on a microscopic scale. In particular, Bernhard *et al.*,[3] using the zero-field muon spin rotation (μSR) technique, searched for any changes in the ferromagnetic signatures with the onset of superconductivity and found none. The spontaneous local field at the apical oxygen site, found in zero-field μSR, remains unchanged through the onset of superconductivity with a continuing weak linear increase down to below 2.5 K. From these measurements, the material was demonstrated to be microscopically uniform with no evidence for spatial phase separation of superconducting and magnetic regions. Similar results are found probing the local field at the Gd site using electron spin resonance (ESR).[4] Hysteresis loops, consistent with ferromagnetism, were observed down to below 5 K in dc magnetization measurements. In addition to the Ru ferromagnetic ordering, μSR and dc magnetization data showed that the Gd sublattice orders antiferromagnetically at $T_N = 2.6$ K. From a fit of Curie-Weiss behavior in the paramagnetic state, effective magnetic moments of 1 and $7\mu_B$ were determined for Ru and Gd, respectively. It was suggested that ferromagnetic ordering of the Ru spins perpendicular to the *c* axis would avoid strong pair breaking effects and enable the coexistence of superconductivity and ferromagnetism. The field of 700 G observed at the muon site was consistent with a dipolar field of in-plane aligned moments. However, subsequent electron-spin-resonance studies showed that the field at the Gd site is 600 G,[4] consistent with a dipolar field arising from moments aligned parallel to the *c* axis. Two things may be said concerning these contradictory results. First, an exchange field must be present in at least one of the sites, and second, because H_{c2} is observed[5] to be large (>100 T) compared to these local fields there is no constraint on alignment direction from the point of view of pair breaking. Measurements of the high-field magnetization were consistent with a saturation magnetization below T_M of $1.2\mu_B$ associated with the Ru moments, consistent with bulk ferromagnetism involving the alignment of all Ru moments.[5] In separate work by Felner *et al.*,[6] two magnetic transitions at 168 and 2.8 K were reported for a nonsuperconducting sample of $RuSr_2GdCu_2O_8$, where the 168-K transition was concluded to be (from ac and dc susceptibility) a transition to antiferromagnetism. It is not as yet clear what are the composition and/or structural differences between Felner's and Tallon's samples.

In this paper, we report temperature-dependent neutron-diffraction results for a $RuSr_2GdCu_2O_8$ sample exhibiting a magnetic transition at 133 K, a superconducting onset transition at 35 K, and a bulk transition at 18 K. We find that the structural parameters vary smoothly as a function of temperature except for the CuO_2 buckling angle and the thickness of the conducting layer (Cu-Cu), which both show sharp

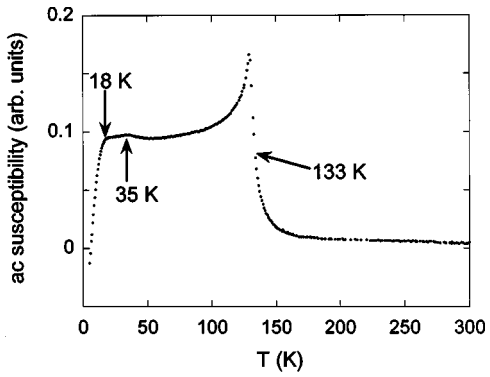

FIG. 1. Ac susceptibility measurement for $RuSr_2GdCu_2O_8$. A ferromagnetic transition at 133 K and a full superconducting transition at 18 K are observed. Superconductivity appears at a higher temperature of ~35 K.

changes in their temperature derivative near T_M. Below the magnetic ordering transition (133 K), we do not observe additional intensity in the 001 reflection, as would be expected for ferromagnetic ordering of Ru moments perpendicular to the *c* axis.

SYNTHESIS AND CHARACTERIZATION

Because of the high absorption cross section (29 400 b) of natural Gd for thermal neutrons, isotopically enriched ^{160}Gd (0.77 b absorption cross section) was used to synthesize a sample for this study. A polycrystalline $RuSr_2{}^{160}GdCu_2O_8$ sample was synthesized by solid-state reaction of RuO_2, $SrCO_3$, $^{160}Gd_2O_3$, and CuO powders. The mixture was first decomposed at 960 °C in air. It was then ground, milled, and die pressed into pellets. The first sintering step took place in a flowing nitrogen atmosphere at 1010 °C. This step results in the formation of a mixture of the precursor material Sr_2GdRuO_6 and Cu_2O and its purpose is to minimize the formation of $SrRuO_3$. The material was then reground and reacted in flowing oxygen for 10 h at 1050 °C. This sintering step was repeated twice with intermediate grinding and milling. Each reaction step was carried out on a MgO single-crystal substrate to prevent reaction with the alumina crucible. Finally, the sample was cooled slowly to room temperature in flowing oxygen.

Figure 1 shows the ac magnetic susceptibility as a function of temperature for the sample used in this study. The magnetic transition previously reported is clearly seen at ~133 K. At lower temperature, superconductivity first appears at 35 K (Fig. 1) and a full superconducting transition is observed near 18 K. Other studies[5] show that the thermodynamic superconducting transition is associated with the higher transition but due to the sample granularity macroscopic screening currents are not established until the lower temperature (18 K).

NEUTRON POWDER DIFFRACTION

Time-of-flight neutron powder diffraction data were collected using all detector banks of the Special Environment Powder Diffractometer at Argonne's Intense Pulsed Neutron Source.[7] To minimize the background, the sample was sealed in a thin-walled aluminum can with helium exchange gas to ensure homogeneous cooling. Diffraction data were acquired at 11 different temperatures between 300 and 12 K using a closed-cycle helium (DISPLEX) refrigerator.

The crystal structure was refined by the Rietveld technique, using the GSAS code[8] and the high resolution backscattering data ($2\theta = 145°$). The refinement included up to 1107 Bragg reflections over the *d*-spacing range 0.5–4 Å. Background, peak width, absorption, and extinction parameters were refined, together with lattice parameters, atom positions, oxygen site occupancies, isotropic temperature factors for the cations, $O1$, $O1'$, and $O2$, and an anisotropic temperature factor for $O4$ (see Table I).

Initial refinements were performed using the average tetragonal $P4/mmm$ structure ($a_p \times a_p \times c$) and starting values obtained from Ref. 2 for the lattice and structural parameters. In this structure, Ru atoms occupy octahedral sites [1(a) at (0 0 0)] and are surrounded by six oxygen atoms [four equatorial atoms ($O1$), and two apical atoms ($O4$)]. Ideally, the equatorial oxygen atoms $O1$ would be at the $2(f)$ sites [at (0 $\frac{1}{2}$ 0)]. However, such a configuration requires an in-plane distance between Ru and $O1$ that is somewhat shorter than expected for Ru^{+5} (Refs. 2 and 3) (~1.919 Å at room temperature) using the ionic size values given by Shannon.[9] Indeed, refinements in this model converged poorly and yielded a large thermal factor of ~7 $Å^2$ for $O1$, indicating that these equatorial oxygen atoms must be displaced off their ideal positions. Excellent refinements were achieved by displacing the $O1$ atoms from the (0 $\frac{1}{2}$ 0) site to new $4(n)$ sites at (~0.12256 $\frac{1}{2}$ 0). For the displaced site, the thermal factor is reduced to a reasonable value of ~0.45 $Å^2$. This displacement corresponds to a rotation of the RuO_6 octahedra by about 13.8° around the *c* axis such that the in-plane Ru-O distance can achieve a physically reasonable value ~1.975 Å. Furthermore, refinements showed that the oxygen occupancy of this site is 1.95(3) (a maximum of two oxygen atoms per unit formula is allowed). Final refinements in this model produced a good fit to the data with agreement factors $R_{wp} = 7.50\%$ and $R_{F^{**}2} = 6.33\%$. Rotation of the RuO_6 octahedra lifts the inversion symmetry of the $O1$ sites with the result that an additional phonon associated with the *c*-axis vibration of this oxygen is evident in the Raman spectra.[10]

When the high-symmetry $P4/mmm$ space group is used to refine the structure with displaced $O1$ sites, multiple $O1$ sites, corresponding to clockwise and counterclockwise rotations of the RuO_6 octahedra, each with nominal 50% occupancy, are defined. In the actual structure, it is unlikely that such disorder would occur on a short length scale because it would require substantial distortion of the corner-sharing RuO_6 octahedra. Rather, one would expect extended ordered regions, at least in the plane perpendicular to the *c* axis, where adjacent RuO_6 octahedra have the opposite sense of rotation. The physical argument for ordering of the rotations along the *c* axis is less clear. However, there is experimental evidence for ordering. Superlattice lines defining a $\sqrt{2}a_p \times \sqrt{2}a_p \times c$ cell have been previously observed in electron diffraction.[11] We also see small superlattice lines in our neutron powder diffraction data (as shown in the inset to Fig. 3).

Based on these observations, we performed additional refinements in the appropriate supercell, using a tetragonal space group $P4/mbm$. The $O1$ oxygen atoms are at $4(g)$ sites (x, $x+\frac{1}{2}$, 0). Figure 2 shows the structure of

TABLE I. Room-temperature structural parameters for $RuSr_2GdCu_2O_8$. In space group $P4/mmm$, Ru is at (0 0 0), Sr at ($\frac{1}{2}$ $\frac{1}{2}$ z), Gd at ($\frac{1}{2}$ $\frac{1}{2}$ $\frac{1}{2}$), Cu at (0 0 z), $O1$ at (x $\frac{1}{2}$ 0), $O2$ at ($\frac{1}{2}$ 0 z), and $O4$ at (0 0 z). In space group $P4/mbm$, Ru is at (0 0 0), Sr at ($\frac{1}{2}$ 0 z), Gd at ($\frac{1}{2}$ 0 $\frac{1}{2}$), Cu at (0 0 z), $O1$ and $O1'$ at (x $x+\frac{1}{2}$ 0), $O2$ at ($\frac{1}{4}$ $\frac{1}{4}$ z), and $O4$ at (0 0 z). Constraints are: $B(O1)=B(O1')$; $x(O1)=x(O1')+\frac{1}{2}$.

		$P4/mmm$	$P4/mbm$	
			$O1$	$O1$ and $O1'$
a (Å)		3.835 99(3)	5.424 92(5)	5.424 91(4)
c (Å)		11.562 8(2)	11.562 6(2)	11.562 8(2)
Volume (Å^3)		170.145(3)	340.284(6)	340.290(6)
Ru	B (Å^2)	0.22(3)	0.23(3)	0.22(3)
Sr	B (Å^2)	0.49(3)	0.54(3)	0.49(3)
	z	0.1903(1)	0.1906(1)	0.1903(1)
^{160}Gd	B (Å^2)	0.07(3)	0.10(3)	0.07(3)
Cu	B (Å^2)	0.14(2)	0.16(2)	0.14(2)
	z	0.3547(1)	0.3547(1)	0.3547(1)
$O1$	B (Å^2)	0.60(6)	0.29(6)	0.59(6)
	x	0.1228(7)	0.1922(4)	0.1888(3)
	n	0.49(1)×4	0.75(1)×4	0.70(1)×4
$O1'$	B (Å^2)			0.59(6)
	x			0.6888(3)
	n			0.27(1)×4
$O2$	B (Å^2)	0.42(2)	0.42(2)	0.42(2)
	z	0.3714(1)	0.3715(1)	0.3714(1)
$O4$	$B_{11}=B_{22}$ (Å^2)	1.14(6)	1.15(6)	1.14(6)
	B_{33} (Å^2)	0.18(7)	0.19(7)	0.19(7)
	z	0.1653(2)	0.1653(2)	0.1653(2)
	R_p (%)	5.09	5.48	5.07
	R_{wp} (%)	7.50	8.14	7.43
	R_{F**2} (%)	6.33	6.55	6.19
	χ^2	2.55	3.00	2.50

$RuSr_2GdCu_2O_8$ in this space group. The results of these refinements are given in Table I. It was immediately obvious from these refinements that the ordering was not complete. When only one oxygen site (i.e., one sense of rotation for the RuO_6 octahedra) was allowed, the $O1$ site occupancy refined to 0.75 (see the middle column of Table I). Excellent refinements were achieved by allowing a second oxygen site, $O1'$, representing a minor fraction of RuO_6 octahedra rotated in the opposite sense (i.e., out of phase with the major fraction).

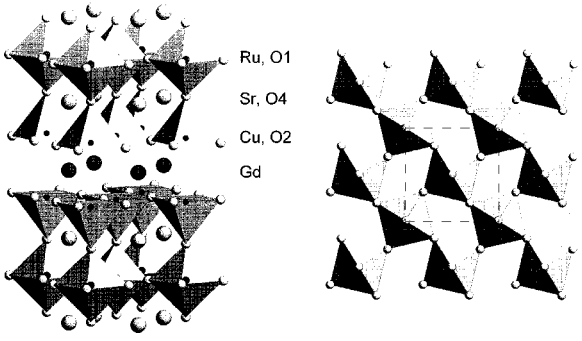

FIG. 2. Structure of $RuSr_2GdCu_2O_8$ in space group P4/mbm (a). A [0 0 1] projection showing the rotation of the RuO_6 octahedra (b).

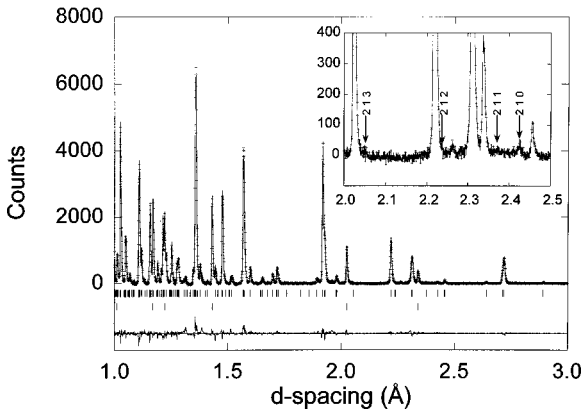

FIG. 3. Best-fit Rietveld refinement profile showing observed (+) and calculated (line) intensities. Cubic aluminum, from the sample holder, was included in the refinements ($Fm3m$, a = 4.048 Å at 300 K). The markers below the profile correspond to the Bragg peak positions for: $RuSr_2GdCu_2O_8$ (top) and aluminum (bottom). The difference between observed and calculated intensities is shown at the bottom. The refined background has been subtracted. Some superlattice reflections are indicated by arrows as shown in the inset.

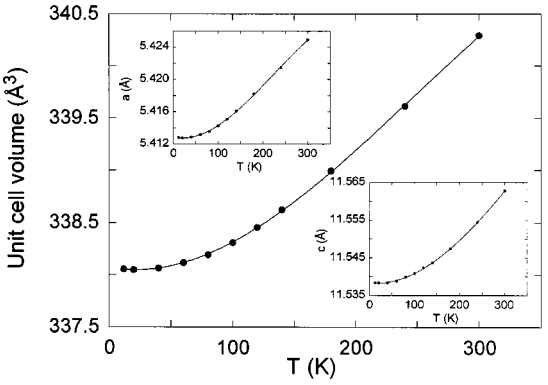

FIG. 4. Unit-cell volume and lattice parameters *a* and *c* (insets) as a function of temperature. The size of the error bars is smaller than the symbols.

With no constraint on the sum, the $O1$ and $O1'$ site occupancies refined to 0.70(1) and 0.27(1), respectively (see last column of Table I), giving a total occupancy of 0.97(2). The success of this unconstrained refinement confirms the validity of the partially ordered model. Figure 3 shows the raw diffraction data and Rietveld refinement profile for this partially ordered model.

Our observation of partial ordering is in agreement with high-resolution transmission electron microscopy (HRTEM) observations of multiple misoriented domains of dimensions 50–200 Å reported by McLaughlin *et al.*[11] The domains are separated by well-defined antiphase boundaries at which the sense of rotation of the RuO_6 octahedra is reversed. We speculate that these domains form upon cooling the material from high temperature. At high temperature it is plausible that thermal motion results in a fully disordered structure. Upon cooling, domains with a particular sense of rotation nucleate and grow. We attribute no special significance to the approximate 75%/25% ordering in our sample. The degree of ordering will likely be different for other samples depending on the annealing conditions.

Ordered distortions of the RuO_6 octahedra, such as shear displacements of the apical, $O4$, oxygen atoms or tilting of the octahedra are conceptually possible and would result in further reduction of the space-group symmetry. For example, one could envision displacement of the two $O4$ apical oxygen atoms of a RuO_6 octahedron in opposite directions with or without a corresponding tilt of the entire octahedron involving displacements of the $O1$ oxygen atoms out of the plane. Such a distortion would give an orthorhombic space group. We attempted refinements with several possible models of this type, but found no evidence for further reduction of the space-group symmetry in our data. The refined atomic displacements defined by such models were within our spatial resolution (<0.1 Å) and any small improvements in *R* values were not statistically justified in terms of the additional complexity of the models. However, it may be useful to revisit such ideas if single-crystal data or powder data of higher resolution become available.

Unit-cell volume and lattice parameters *a* and *c* (Fig. 4 and insets) are plotted as a function of temperature. No sign of any anomaly (within our instrumental resolution) suggestive of a lattice magnetostriction in the vicinity of the ferromagnetic transition is observed. A smooth decrease is seen

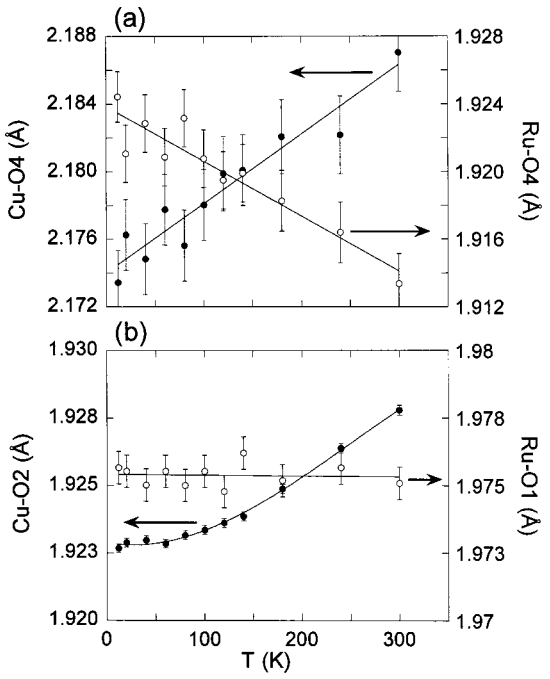

FIG. 5. Cu-O4 and Ru-O4 bond-lengths (a) and Cu-O2 and Ru-O1 bond lengths (b) vs temperature.

upon cooling from 300 to 12 K. Selected bond lengths for the Ru-O and Cu-O bonds are plotted in Fig. 5. Interestingly, the equatorial Ru-O1 bond length remains unchanged with decreasing temperature while the apical Ru-O4 bond length exhibits a negative thermal expansion and increases monotonically upon cooling. The magnitude of this increase ($\sim$0.01 Å) is compensated by the shortening, by about the same magnitude, of the Cu-O4 bond length [Fig. 5(a)] resulting in almost unchanged thickness of the blocking layer (the Ru-Cu) block shrinks by only $\sim$ 0.004 Å between 300 and 12 K. On the other hand, we find that the RuO_6 octahedra rotate further with decreasing temperature so that the Ru-O1 bond length remains nominally ''constant.'' Figure 6 shows the linear relation between the rotation angle of the RuO_6 octahedra and temperature.

The thermal expansion coefficient for the thickness of the conducting block (the Cu-Cu distance) changes abruptly at the ferromagnetic transition temperature, as shown in Fig. 7. Above T_M, this coefficient is more than three times larger

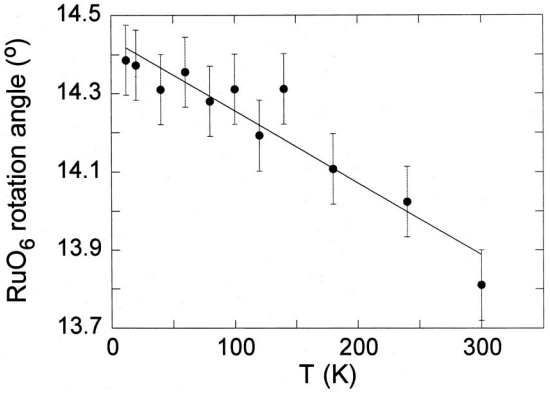

FIG. 6. Rotation angle of the RuO_6 octahedra about the *c* axis as a function of temperature.

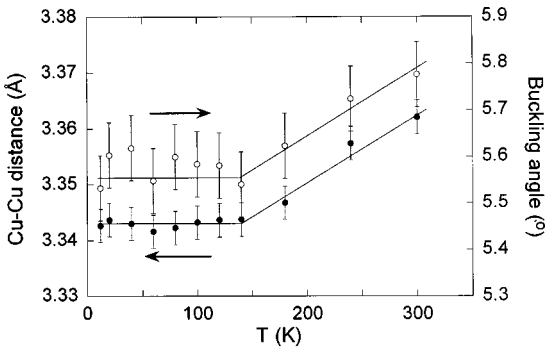

FIG. 7. Cu-Cu bond-length (between two adjacent CuO_2 planes) and CuO_2 buckling angle (defined as the angle at which O2 atoms stick out of the Cu plane) vs temperature. Both curves show an anomaly around 133 K at which the sample becomes ferromagnetic.

than the thermal expansion coefficient of the *c* axis. Below T_M, no significant variation is observed. In a similar way, the buckling angle of the CuO_2 layers (also shown in Fig. 7) exhibits two distinct linear responses to temperature. Hence the thickness and the buckling of the conducting block conspicuously respond to a charge redistribution that is taking place near the transition to ferromagnetism. This observation, that the magnetic transition involving the Ru sites produces a structural response in the CuO_2 planes, might suggest some degree of hybridization of the Ru and Cu electronic states. An alternative, but less likely, explanation is that the spontaneous field might partially (perhaps dynamically) align spins in the CuO_2 layer, giving rise to the structural response.

SEARCH FOR FERROMAGNETISM OF THE Ru SUBLATTICE

In neutron diffraction, ferromagnetism is manifested as additional scattering for specific peaks that have nuclear scattering intensity. In the present study, the sharply decreasing form factor for Ru^{5+} and the large nuclear intensity for most peaks makes it feasible to observe magnetic scattering only for the 001 peak. (We conclude from bond lengths that Ru is in the 5+ state, but note that the form factor for Ru^{4+} is not significantly different than that for Ru^{5+}). The $Ru^{5+}(4d^3)$ is a large ion and its form factor decreases sharply with $\sin\theta/\lambda(=1/2d)$. Using the known form factors for $4d^8$, $4d^7$, $4d^5$, and $4d^4$ (Ref. 12) we have estimated the form factor for the Ru^{5+} ion and found that the magnetic contribution to the neutron intensities for the 001, 002, 003/010, and 004 reflections are ~86, 53, 27, and 10% of their full value. The nuclear intensity of the 001 reflection is accidentally rather small (Fig. 8) and we have estimated a 28% intensity increase (after correction for the form factor) in the case of ferromagnetism due to ordering of the Ru moments perpendicular to the *c* axis with $1\mu_B$/Ru (low spin state). This is the ferromagnetic ordering initially proposed to be most likely.[3]

To maximize the signal-to-noise ratio, a specially made aluminum can was used (length, diameter, and wall thickness equal to $1\frac{1}{2}$, $\frac{1}{4}$, and 0.005 in.). Neutron data were collected for 10 h at 300 K, 12 h at 12 K, and for 8 h at each of the following temperatures: 20, 40, 60, 80, 100, 120, 140, 180,

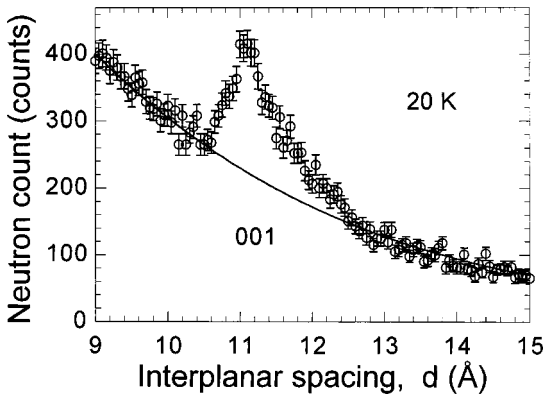

FIG. 8. Observed pattern of the 001 reflection at 20 K. Data collection time was 8 h. The function $A\cdot d\cdot e^{(-d/B)}$, where *A* and *B* were refined [1328(48) and 2.65(3)], was used to fit the background (solid line).

and 240 K. A typical profile of the raw data near the 001 reflection, collected at the $2\theta\sim14.6°$ detector bank, is shown in Fig. 8. The observed background (sample in aluminum can) is about half of the background obtained with the standard vanadium can and is mostly due to paramagnetic scattering from the Gd ionic spins (see below).

The background was fitted to the function (solid line in Fig. 8) $A\cdot d\cdot e^{-(d/B)}$, where *d* is the interplanar spacing and *A* and *B* were refined for each temperature. A plot of the background count vs temperature (Fig. 9) shows a sharp decrease in the background count as the sample is cooled below ~ 30 K. We believe that this decrease is related to fluctuations of the spins of the Gd ions as the ordering temperature is approached. The background from paramagnetic scattering decreases significantly as Gd spins begin to order.

The integrated neutron count (INC) in the 001 reflection was obtained for each temperature, after subtracting the fitted background and normalizing to the total upstream monitor count, and is plotted vs temperature in Fig. 10. These results were found to be insensitive to the choice of background function, *d* range of integration and other modes of normalization (e.g., normalization with respect to the proper time of flight band in the monitor). The estimated increase in the INC of the 001 reflection due to $1\mu_B$/Ru (28%) and $0.5\mu_B$/Ru (7%) are also shown (Fig. 10, arrows). Our results

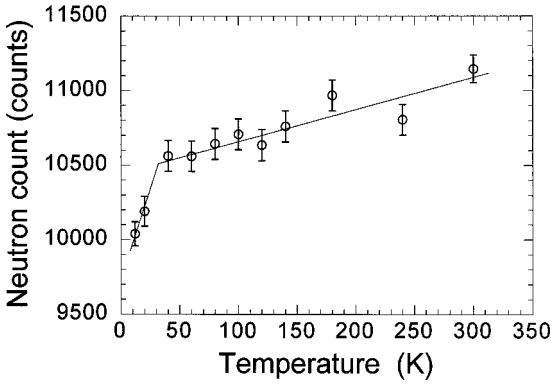

FIG. 9. The integrated neutron count (INC) in the background of 001 (normalized by the total monitor counts) as a function of temperature.

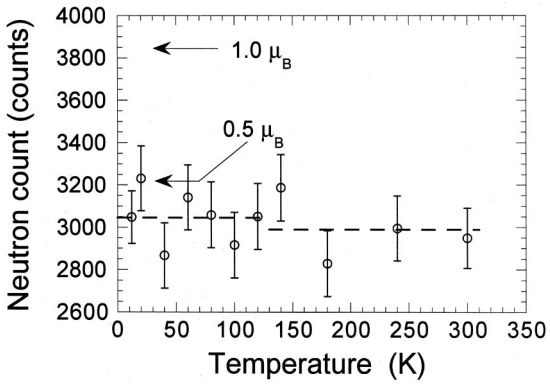

FIG. 10. Observed INC in the 001 reflection as a function of temperature. The two horizontal dashed lines represent the mean INC below and above 130 K.

(Fig. 10), do not show the expected change in the INC that would indicate full ferromagnetic ordering of the Ru moments below 133 K. Due to the experimental uncertainty, however, we note that any INC increase due to $\mu_\perp$ less than about $0.3\mu_B$/Ru may be too small to be unambiguously observed in this measurement.

Hence, from our measurements, there is no evidence for a ferromagnetic component perpendicular to the *c* axis. The statistics of our measurement allow us to say that the ordered in-plane ferromagnetic moment cannot be larger than about $0.3\mu_B$. We recall that the saturation magnetization indicated an effective moment of $1.2\mu_B$.[5] Our accuracy for this measurement is limited mainly by the large background resulting from paramagnetic scattering from the Gd spins. Thus the best opportunity for observing ferromagnetic scattering on top of the nuclear scattering is for the 001 reflection, where the nuclear scattering is accidentally small. There is little chance of observing magnetic scattering for other peaks, where the nuclear scattering is much larger and the expected magnetic scattering is even smaller because of the form factor. For these reasons, it is difficult to test for other magnetic structures, such as ferromagnetic ordering along the *c* axis or antiferromagnetic ordering. We searched our data for any other new peaks at low temperature that might come from antiferromagnetic ordering and found none. However, it is unlikely that such peaks would be seen in our measurement, given the sharply decreasing form factor.

CONCLUSIONS

We have shown that $RuSr_2GdCu_2O_8$ has a modified $YBa_2Cu_3O_7$-type structure in which the unit cell has been enlarged to $\sqrt{2}a_p \times \sqrt{2}a_p \times c$ as a result of coordinated rotations of the RuO_6 octahedra which substitute for the Cu-O chains. These rotations are required to accommodate a reasonable in-plane Ru-O bond length. We see no additional structural distortions, such as shear displacements of the apical oxygen atoms ($O4$) of the type that occur when ReO_6 octahedra are substituted at the Hg sites in $(Hg, Re)Sr_2Ca_{n-1}Cu_nO_z$.[13] The sample contains domains of opposite sense of RuO_6 rotation separated by antiphase boundaries. The sense of rotation is completely ordered within a domain. In an unconstrained Rietveld refinement, we observe a fraction of 0.70(1) rotated in one direction and a fraction of 0.27(1) rotated in the opposite direction. These fractions are the fractional populations of the two domains. We speculate that these populations are likely to depend on the annealing of the sample. A quenched sample would be likely to show nominally equal populations in the two domains, while a well annealed sample may approach a single domain in each crystallite. This conclusion has important implications for the dependence of superconducting properties on annealing. Tallon and co-workers[2,5] have shown that resistive and thermodynamic superconducting transitions are seen in all samples, but macroscopic superconductivity (as probed by magnetic susceptibility) is only observed in properly annealed samples. One could conclude that macroscopic screening currents are established only when there has been sufficient annealing to allow the ordered domains to grow to a critical size. The antiphase boundaries which separate the ordered domains apparently disrupt superconductivity.

The scattering from ferromagnetism, below 133 K, involving full ordering of Ru moments in the plane perpendicular to the *c* axis would be readily seen in our experiments. However, we do not see the expected scattering. Other models for the magnetic structure would be consistent with this result. These include: ferromagnetism along the *c* axis, weak ferromagnetism (i.e., canted antiferromagnetism)[14] of the Ru planes, or itinerant ferromagnetism as has been reported for $SrRuO_3$.[15] Our measurements are not sensitive to an in-plane ordered moment on the Ru sites smaller than about $0.3\mu_B$ because the signal-to-noise ratio of the measurement is limited by the large paramagnetic scattering from Gd.

We observe a curious structural response at the magnetic ordering transition, 133 K. The temperature dependence of the Cu-Cu distance (the thickness of the CuO_2 double layer) and the buckling angle of the CuO_2 planes changes abruptly at this temperature. It is surprising that such a structural response is seen in the CuO_2 planes rather than in the RuO_6 octahedra, which have several degrees of freedom that could be sensitive to subtle changes in bonding resulting from the spin ordering. We speculate that the energy levels for Ru and Cu are very similar and may be thought of as forming a narrow band. If such a hypothesis is true, an active charge transfer between Ru and Cu atoms could be observed similar to what is seen in Fig. 5(a). This is in agreement with magnetoresistance measurements by McCrone, Cooper, and Tallon[16] indicating a strong exchange interaction ($J = 35$ meV) between the spins and the carriers. Because this is comparable to the superconducting energy gap one would expect suppression of superconductivity due to exchange if the carriers are only on the CuO_2 planes. It is therefore concluded that the carriers are associated with both CuO_2 and RuO_6 bands (i.e., itinerant ferromagnetism). Because of the itinerant nature of the Ru moments, anomalies due to magnetic ordering could be manifest in the CuO_2 planes rather than in the RuO_6 octahedra. An alternative explanation that it is the Cu spins which order ferromagnetically has to be dismissed as highly unlikely. Zn substitution for Cu rapidly suppresses T_C while having little effect on T_M.[5]

ACKNOWLEDGMENTS

We are grateful to Dr. Christian Bernhard (Max Planck Institüt) for procuring the ^{160}Gd for the present sample. This

work was supported by the ARPA/ONR at NIU and by the National Science Foundation, Office of Science and Technology Centers under Grant No. DMR 91-20000 (O.C.), the U.S. Department of Energy, Division of Basic Energy Science–Materials Sciences, under Contract No. W-31-109-ENG-38 (J.D.J. and the operation of IPNS), and Ben-Gurion University of the Negev (H.S.). Additional support (J.L.T.) was from New Zealand Marsden.

*Permanent address: Department of Physics, Ben Gurion University of the Negev, P.O. Box 653, Beer Sheva 84190, Israel.

[1] L. Bauernfeind, W. Widder, and H. F. Braun, Physica C **254**, 151 (1995).

[2] J. L. Tallon, C. Bernhard, M. E. Bowden, P. W. Gilberd, T. M. Stoto, and D. J. Pringle, IEEE Trans. Appl. Supercond. **9**, 1696 (1999).

[3] C. Bernhard, J. L. Tallon, Ch. Niedermayer, Th. Blasius, A. Golnik, E. Brucher, R. K. Kremer, D. R. Noakes, C. E. Stonach, and E. J. Ansaldo, Phys. Rev. B **59**, 14 099 (1999).

[4] A. Fainstein, E. Winkler, A. Butera, and J. L. Tallon, Phys. Rev. B **60**, R12 597 (1999).

[5] J. L. Tallon, C. Bernhard, and J. W. Loram, J. Low Temp. Phys. (to be published).

[6] I. Felner, U. Asaf, S. Reich, and Y. Tsabba, Physica C **311**, 163 (1999).

[7] J. D. Jorgensen, J. Faber, Jr., J. M. Carpenter, R. K. Crawford, J. R. Haumann, R. L. Hitterman, R. Kleb, G. E. Ostrowski, F. J. Rotella, and T. G. Worlton, J. Appl. Crystallogr. **22**, 321 (1989).

[8] A. C. Larson and R. B. Von Dreele, GENERAL STRUCTURE ANALYSIS SYSTEM, University of California (1985–1990).

[9] R. D. Shannon, Acta Crystallogr., Sect. A: Cryst. Phys., Diffr., Theor. Gen. Crystallogr. **A32**, 751 (1976).

[10] D. J. Pringle, J. L. Tallon, B. G. Walker, and H. J. Trodahl, Phys. Rev. B **59**, R11 679 (1999).

[11] A. C. McLaughlin, W. Zhou, J. P. Attfield, A. N. Fitch, and J. L. Tallon, Phys. Rev. B **60**, 7512 (1999).

[12] *International Tables for Crystallography C*, edited by E. J. C. Wilson (Kluwer Academic, Dordrecht, 1992), p. 391.

[13] O. Chmaissem, J. D. Jorgensen, K. Yamaura, Z. Hiroi, M. Takano, J. Shimoyama, and K. Kishio, Phys. Rev. B **53**, 14 647 (1996).

[14] Ferromagnetism along *y* is compatible with antiferromagnetism along *x* (both belong to the magnetic space group Pb′am′.) W. Opechowski and R. Guccione, in *Magnetism*, edited by G. T. Rado and H. Suhl (Academic, New York, 1965), Vol. IIA, p. 105, so that a canted antiferromagnet (a weak ferromagnet) is possible.

[15] J. M. Longo, P. M. Raccah, and J. B. Goodenough, J. Appl. Phys. **39**, 1327 (1968).

[16] J. E. McCrone, J. R. Cooper, and J. L. Tallon, J. Low Temp. Phys. (to be published).